Earth and Planetary Science Letters 275 (2008) 70–79

Contents lists available at ScienceDirect

Earth and Planetary Science Letters

journal homepage: www.elsevier.com/locate/epsl

The effect of bulk composition and temperature on mantle seismic structure

Wenbo Xu [a], Carolina Lithgow-Bertelloni [b,*], Lars Stixrude [b], Jeroen Ritsema [a]

[a] Department of Geological Sciences, University of Michigan, Ann Arbor, MI 48109, USA
[b] Department of Earth Sciences, University College London, Gower Street, WC1E 6BT, London, United Kingdom

ARTICLE INFO

Article history:
Received 29 October 2007
Received in revised form 1 August 2008
Accepted 5 August 2008
Available online 19 September 2008

Editor: R.W. Carlson

Keywords:
mantle composition
mechanical mixture
equilibrium assemblage
mantle discontinuity
transition zone
shear velocity

ABSTRACT

We use a self-consistent thermodynamic formalism to compute the phase equilibria and physical properties of model mantle compositions, demonstrating that the seismological properties of a mantle comprised of (1) an equilibrium assemblage (EA) of pyrolitic composition and (2) a mechanical mixture (MM) of basalt and harzburgite with identical bulk composition differ significantly. We calculate the density, compressional wave velocity (V_P), and shear wave velocity (V_S) of EA and MM with basalt fraction varying from 0% to 100% and along adiabats with potential temperatures ranging from 1000 K to 2000 K. For MM, V_S in the transition zone is greater, increases more rapidly with depth, and is insensitive to basalt fraction, while for EA V_S decreases by 2.5% with increasing basalt fraction for fractions <70%. The magnitude and sharpness of the 520-km discontinuity depends strongly on temperature in both EA and MM, which may explain lateral variations in its seismic detection. Both MM and EA feature complex structure in the depth range 640–750 km due to the transformations of akimotoite, ringwoodite, and garnet to denser assemblages. MM is faster than most seismological models in the upper mantle, and slower in the lower mantle, suggesting an increase of basalt fraction with depth in the mantle.

1. Introduction

At mid-ocean ridges, partial melting generates a basaltic crust and leaves behind its depleted complement, harzburgite. The oceanic lithosphere thus formed is physically and chemically layered. What is the fate of this chemical heterogeneity, which is continuously injected into the mantle during subduction (Fig. 1)? Do basalt and harzburgite equilibrate chemically as pyrolite? If they do, over what time scales? If not, should we consider the mantle as a non-equilibrated mechanical mixture of basalt and harzburgite?

Experiments have shown that a homogeneous pyrolite source region can explain the observed composition of mid-ocean ridge basalt (Chen et al., 1991; Frey et al., 1978; McKenzie and Bickle, 1988) and the seismic velocity profile of upper mantle and transition zone to first order (Irifune, 1993; Ita and Stixrude, 1992; Ringwood, 1979; Weidner, 1985). Indeed, nearly all mineralogical models, upon which comparisons to seismology are based, view the mantle as homogeneous and pyrolitic (Bass, 1995; Francis, 1987; Ringwood, 1966, 1969) or chemically stratified with homogeneous and equilibrated compositions in each layer (e.g. Anderson and Bass, 1986; Mattern et al., 2005). However, the assumption of major element chemical equilibrium appears at odds with the small chemical diffusivity of mantle materials (10^{-14}–10^{-16} m^2 s^{-1}) in the solid-state (Hoffman and Hart, 1978; Farber et al., 1994; Yamazaki et al., 2000). On the other hand, partial melting, a free fluid phase or grain-size reduction at reconstructive phase transformations may increase the rate of equilibration (Hoffman and Hart, 1978; Ito and Sato, 1991).

Mechanically mixed mantle models have been considered as well (Hoffman and Hart, 1978; Allégre and Turcotte, 1986). Allégre and Turcotte (1986) suggested a marble cake structure for the mantle in which subducted oceanic lithosphere is deformed into pervasive, narrow pyroxenite veins. Mantle convection simulations suggest a heterogeneous mantle made of a mechanical mixture of basalt and harzburgite (Brandenburg and Van Keken, 2007; Christensen and Hofmann, 1994; Davies, 2006; Nakagawa and Buffett, 2005; Xie and Tackley, 2004). A stirring time of the mantle between 250 and 750 Ma (Kellogg et al., 2002) limits the amount of stretching and folding of subducted heterogeneity that can occur in the mantle over the age of the Earth. It seems thus implausible to fully equilibrate subducted basalt and harzburgite into pyrolite. Some dynamical models further show large scale segregation of basalt from harzburgite, the details of which depend sensitively on the assumed density contrast between the two lithologies as a function of depth. In our view the unique properties of a mechanically mixed mantle do not depend on whether basalt and harzburgite fractions segregate from one another, only that the lithologic integrity of the subducted basalt and harzburgite be preserved for geologically significant times. We

* Corresponding author. Tel.: +44 20 7679 2363; fax: +44 20 7679 2433.
E-mail address: c.lithgow-bertelloni@ucl.ac.uk (C. Lithgow-Bertelloni).

0012-821X/$ – see front matter © 2008 Elsevier B.V. All rights reserved.
doi:10.1016/j.epsl.2008.08.012

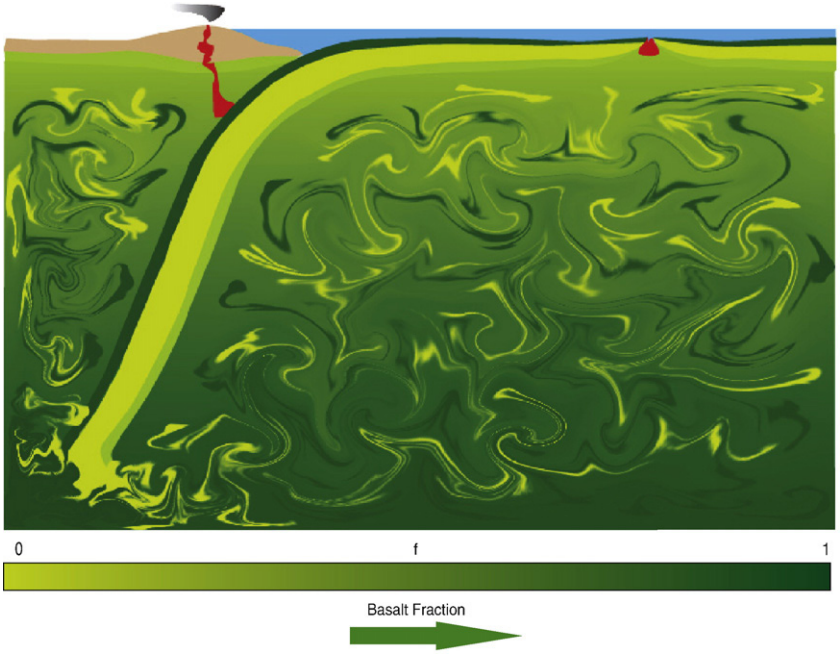

Fig. 1. Dynamic and chemical processes near (right) a mid-ocean ridge and (left) a subduction zone. At mid-ocean ridges, because of decompression partial melting, upwelling peridotite (medium green) forms two different chemical layers, basalt (dark green) and the complementary residual harzburgite (light green). At subduction zones, the differentiated oceanic crust subducts into the mantle. Density contrasts between basalt and harzburgite may drive segregation. The end result may be a mantle that is mechanically mixed, with basalt preferentially accumulating in the lower mantle and harzburgite in the upper mantle. (For interpretation of the references to color in this figure legend, the reader is referred to the web version of this article.)

further speculate on the possible consequences of segregation of basalt and harzburgite, which could produce radial or lateral variations in bulk composition.

In this paper, we explore the effects of major element disequilibrium on seismological properties of the mantle. We demonstrate that even with identical bulk compositions, an equilibrium assemblage along the basalt-harzburgite join and a mechanical mixture of basalt and harzburgite have different phase equilibria and therefore different seismic velocities. We explore the influence of potential temperature and bulk composition, using the relative proportions of basalt and harzburgite (the basalt fraction) as a compositional metric. We consider two end-member models for combining basalt and harzburgite fractions in the mantle: (1) the Equilibrium Assemblage (EA) with perfect equilibration and (2) the Mechanical Mixture (MM) with perfect disequilibrium between the two fractions.

We compute the seismic velocities of EA and MM following the self-consistent thermodynamic model developed by Stixrude and Lithgow-Bertelloni (2005a,b). We focus in particular on shear wave velocities (V_S), which is most sensitive to our mineralogical parameters and which is best constrained by a combination of travel-time, surface wave and normal mode data.

2. Methodology

2.1. Compositional model

The phase assemblages for EA

$$\phi[f\boldsymbol{X}_B + (1-f)\boldsymbol{X}_H] \tag{1}$$

and MM

$$f\phi[\boldsymbol{X}_B] + (1-f)\phi[\boldsymbol{X}_H] \tag{2}$$

with identical bulk compositions are significantly different, where $\boldsymbol{\phi}$ is the vector of phase proportions, $\boldsymbol{X}$ is the vector defining the bulk composition, subscripts B and H refer to basalt and harzburgite respectively, and f is the basalt fraction.

In this study, we explore a variety of bulk compositions represented by the basalt fraction f, in the equilibrium Eq. (1) and disequilibrium Eq. (2) limits. We focus on a simplified model of mantle composition with six components: CaO, FeO, Na_2O, Al_2O_3, MgO, SiO_2, 20 phases, and 46 mantle species, an updated version of Stixrude and Lithgow-Bertelloni (2005b) (Tables 1 and 2 in the Appendix). We take as our reference estimate of the bulk composition of the mantle the Depleted Mid-Ocean-Ridge-Basalt Mantle (DMM) of Workman and Hart (2005). As most basalt produced on Earth is at mid-ocean ridges, our choice of basalt composition is meant to be representative of average oceanic crust rather than the smaller volume produced in settings that may be influenced by hotspot and arc magmatism. Hence, we approximate the composition of basalt, $\boldsymbol{X}_B$ as the primary N-MORB, from average glass compositions, of Presnall and Hoover (1987); the same composition used in the study of Workman and Hart (2005). We have confirmed that variations in MORB compositions alter physical properties insignificantly: the shear wave velocity of the DSDP3-18 basaltic glass of Green et al. (1979) differs from that of our composition by less than 0.01 km/s. We use a harzburgite model, $\boldsymbol{X}_H$, which is the most depleted composition of abyssal peridotites from Baker and Beckett (1999) (Table 1). Because the harzburgite composition is not in perfect mass balance with the DMM and MORB compositional models, we slightly modify the harzburgite composition to achieve mass balance, and determine the basalt fraction f_P that produces the DMM composition, $\boldsymbol{X}_P$ such that

$$\boldsymbol{X}_P = f_P\boldsymbol{X}_B + (1-f_P)\boldsymbol{X}_H^* \tag{3}$$

is exactly satisfied and the quantity

$$\varepsilon\left(f_P, \boldsymbol{X}_H^*\right) = \sum_j^{\text{phase}} \left[\phi_j(\boldsymbol{X}_H) - \phi_j\left(\boldsymbol{X}_H^*\right)\right]^2 \tag{4}$$

is minimized at 0 GPa, and 1600 K, where $\boldsymbol{X}_H^*$ is our modified harzburgite composition. The modifications to the harzburgite

Table 1
Bulk composition in mol%

Component	Pyrolite[a]	Basalt[a]	Harzburgite[b]	Modified harzburgite[c]
SiO_2	38.71	51.75	36.07	36.04
MgO	49.85	14.94	56.51	56.54
FeO	6.17	7.06	6.07	5.97
CaO	2.94	13.88	0.81	0.79
Al_2O_3	2.22	10.19	0.53	0.65
Na_2O	0.11	2.18	0.00	0.00

[a] Workman and Hart, 2005.
[b] Baker and Beckett, 1999.
[c] Modified Harzburgite under mass and phase balance.

composition amount to less than 1 mol% for all components (Table 1) and change the seismic wave velocity by less than 0.01 km/s.

We find from this analysis that the basalt fraction of the mantle f_P=18%. A similar value is found from a simple analysis of tectonic rates. Assuming that: 1) the oceanic crust is 7 km thick, 2) the Cenozoic mean value of the rate of subduction of 3.35 km^2/yr (Xu et al., 2006) is representative of the last 4.6 Ga of Earth's history, 3) the entire mantle has been differentiated at least once, and 4) equilibration is inefficient, we find a basalt fraction of 12%. A similar analysis (Morgan and Morgan, 1999) found f_P~20% by considering greater tectonic rates in the past. MORB compositions also suggest a significant fraction of recycled oceanic crust in the MORB source (Hirschmann and Stolper, 1996). Petrological estimates based on olivine phenocryst compositions suggest f_P=2–20% (Sobolev et al., 2007).

2.2. Thermodynamic method

We apply a newly developed thermodynamic, petrologic formalism (Stixrude and Lithgow-Bertelloni, 2005a,b), which enables self-consistent computations of physical properties, phase equilibria, and mantle isentropes. This model uses the concepts of fundamental thermodynamic relations (Callen, 1960) and Legendre transformations to capture complete information of all equilibrium states in a single functional form. Generalization of the usual isotropic thermodynamics to conditions of anisotropic stress and strain permit self-consistent computation of the full elastic constant tensor, including the bulk and shear moduli, and therefore the longitudinal and shear seismic wave velocities, V_P and V_S, respectively.

Our calculations consist of three steps. We compute: (1) the equilibrium phase assemblage: the amounts and compositions of coexisting phases by minimizing the Gibbs free energy with respect to the amounts of species at fixed temperature, pressure, and bulk composition, (2) the physical properties of individual phases in the equilibrium assemblage via stress and temperature derivatives of the Gibbs free energy, and (3) the elastic properties of the assemblage as the Voigt–Reuss–Hill average (Watt et al., 1976). For MM steps (1–3) are carried out for basalt and harzburgite compositions separately and, in a fourth step the elastic properties of the aggregate are determined via a Voigt–Reuss–Hill average of the components (basalt and harzburgite) of the mixture. To focus on the influence of bulk composition and major element disequilibrium, we do not include the effects of attenuation, i.e. velocities are in the infinite frequency, elastic limit.

We report phase proportions in terms of atomic fractions

$$\Psi_i = \frac{n_i \phi_i}{\sum_{i}^{20} n_i \phi_i} \tag{5}$$

where, n_i is the number of atoms in the formula unit of phase i. We prefer this measure to mole fraction, which depends on the choice of formula, and because the atomic fraction, unlike the mass or volume fraction, of the olivine polymorphs is unchanged across the olivine to wadsleyite to ringwoodite transformations. We find that atomic, mass and volume fractions are very similar to one another across the range explored here, differing by less than a few percent because the mean atomic weight and volume per atom of coexisting mantle phases are similar to one another.

3. Results

3.1. Influence of disequilibrium

Models EA and MM yield different phase equilibria for the same bulk composition (Fig. 2). The amount of olivine at low pressure in EA is ~60%, while it is 66% in MM. Stishovite appears in MM, but is absent from EA along the 1600 K adiabat. The garnet-pyroxene fraction is less in MM. The influence of disequilibrium can be further understood by considering the variation of phase proportions with f at 300 km depth (Fig. 2, bottom). In the case of MM, stishovite is present at all non-zero values of f because it is stable in the basalt fraction, while in EA stishovite is not stabilized until f exceeds 70%. The differences between MM and EA can be cast schematically as the reaction

$$MgSiO_3(EA) = Mg_2SiO_4(Hz) + SiO_2(Bs)$$

where the right hand side represents the harzburgite (Hz) and basalt (Bs) fractions of the mechanical mixture with more olivine and free silica and less pyroxene than in the equilibrium assemblage.

Since the phase equilibria differ, the seismic velocity of EA and MM are not the same (Figs. 2–4). Tables of computed values of V_P, V_S, and density for EA and MM as a function of basalt fraction and temperature may be found in the supplementary material (Table 3 in the Appendix). Both the compressional (~0.04 km/s) and the shear wave velocity (~0.06 km/s) of MM are higher than that of EA in the transition zone due to the lower proportion of low-velocity phases, such as clinopyroxene (cpx) and the presence of stishovite, a high-velocity mantle phase. The velocity profiles of MM have a greater radial gradient than EA in the deeper transition zone because of the relatively high proportions of wadsleyite, and ringwoodite and the relatively low proportion of garnet. Note that the shallowest portions of EA and MM profiles are fictive as melt forms along the 1600 K adiabat, and are included for completeness.

The discontinuity structures in the EA and MM models differ as well. While EA and MM both show a discontinuity at a depth similar to the Hales discontinuity (60 km), their origin is different. In EA it is due to the spinel to garnet facies transition, whereas in MM it is due to the basalt to eclogite transition in the basaltic fraction of MM. A discontinuity appears near 340 km depth in both models due to the opx-C2/c transition. The transition from coesite to stishovite in MM produces a velocity discontinuity at 310 km depth. The transitions in the pyroxene and silica phases both occur at depths similar to those of the X discontinuity (Revenaugh and Jordan, 1991b; Woodland, 1998; Williams and Revenaugh, 2005).

The depth and velocity contrast of the 410 and 660 km discontinuities are similar in EA and MM, although the latter has somewhat greater velocity contrasts at both discontinuities, due to the greater olivine fraction. In agreement with recent observations of reflected and converted phases (Lawrence and Shearer, 2006) our results show a 660 km discontinuity nearly 3 times narrower than the 410 km discontinuity. The 520 km discontinuity is more prominent in MM due to the larger proportion of wadsleyite and ringwoodite, as compared with EA. The high-velocity gradient immediately deeper than 660 km in EA is due to the gradual transformation of garnet to perovskite. This structure is absent in MM, which has a lesser proportion of garnet at this depth. MM shows an additional velocity discontinuity near 770 km that is due to the transformation of garnet to perovskite and Calcium-ferrite structures.

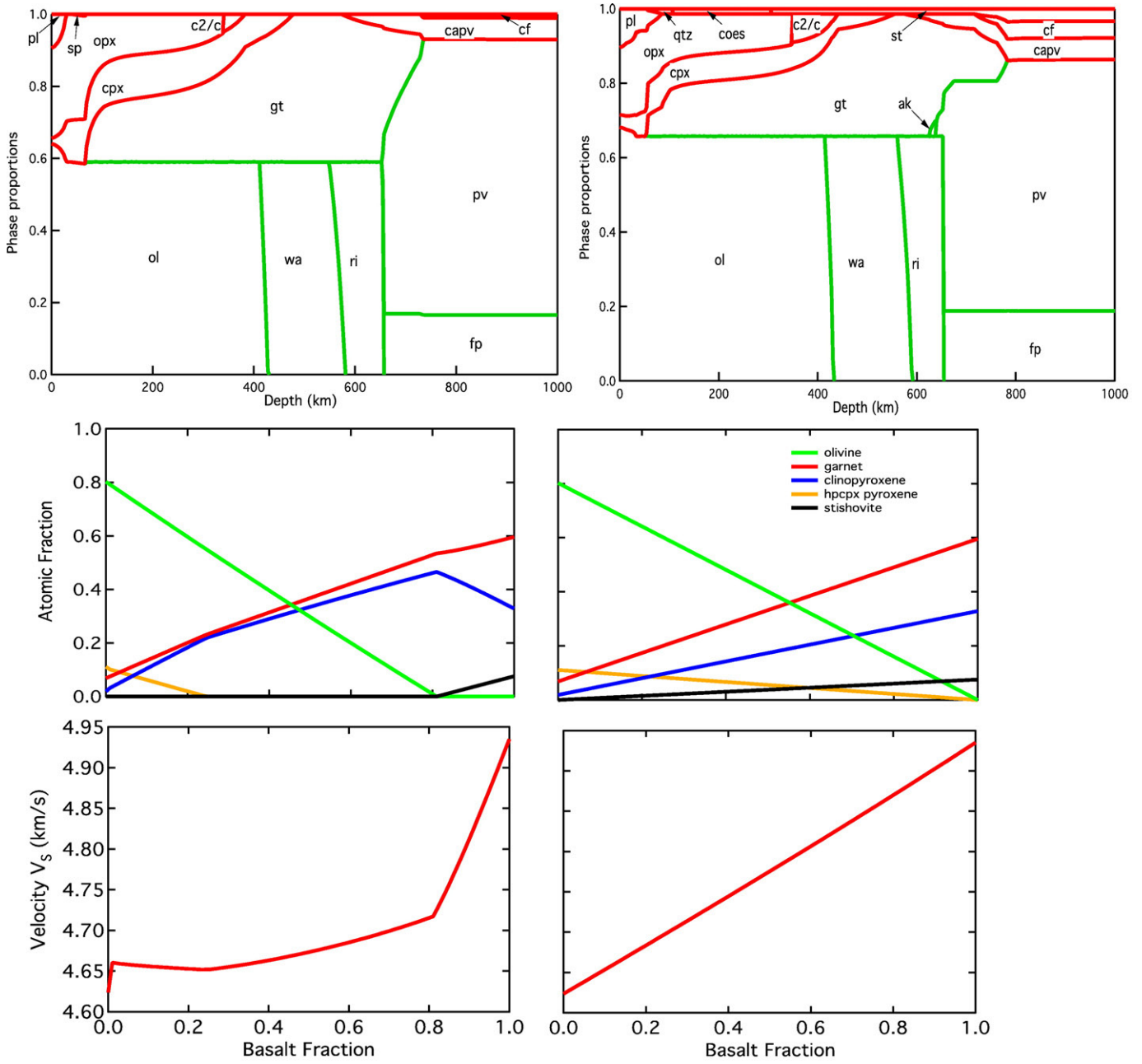

Fig. 2. Phase proportions (top) and variations of V_S and phase proportions at 10 GPa (300 km depth) and 1600 K (bottom) in EA (left) and MM (right) for a pyrolitic bulk composition (Table 1, f=0.18). Phases are: plagioclase (plg), spinel (sp), garnet (gt), olivine (ol), wadsleyite (wa), ringwoodite (ri), orthopyroxene (opx), clinopyroxene (cpx), high pressure Mg-rich clinopyroxene (C2/c), akimotoite (ak), quartz (qtz), coesite (coes), stishovite (st), Ca-silicate perovskite (capv), Mg-rich silicate perovskite (pv), ferropericlase (fp), and Ca-ferrite structured phase (cf). Phase proportions in the bottom panel are for olivine (green), garnet (red), cpx (blue), C2/c (gold), and st (black). (For interpretation of the references to color in this figure legend, the reader is referred to the web version of this article.)

3.2. Influence of bulk composition

In EA, V_S increases with increasing basalt fraction except in the transition zone, at depths shallower than 80 km, and between 660–750 km (Fig. 5). In the transition zone, with increasing f V_S in the transition zone first decreases (f<70%) and then increases (f>70%) as function of basalt fraction. The velocity varies non-linearly with basalt fraction, so that the compositional derivative dV_S/df, where f is basalt fraction, is a strong function of bulk composition. These variations can readily be understood on the basis of the phase equilibria: as basalt fraction increases, the proportion of olivine (a relatively low-velocity phase) decreases, while the proportion of garnet (a relatively high-velocity phase) increases. In the transition zone, olivine transforms into wadsleyite and ringwoodite, both of which are faster than garnet. Especially when the basalt fraction exceeds 70%, not only is stishovite (fast phase) stabilized but its proportion grows.

The depth and thickness of discontinuities vary with composition: in EA the 410 km discontinuity is slightly shallower (by 10 km) and substantially sharper (17 vs. 11 km, respectively) when basalt fraction f is increased from 0 to 0.4. The shallowing is due to the increasing iron content with increasing f (from X_{Fe}=Fe/(Fe+Mg)=9.6% to 13.5%), which tends to stabilize wadsleyite to lower pressures at the expense of olivine. The increase in iron fraction, combined with the influence of partitioning among transforming and non-transforming phases (Stixrude, 1997) accounts for the change in sharpness. The transition near 410 km depth disappears completely for f>80% as olivine is no

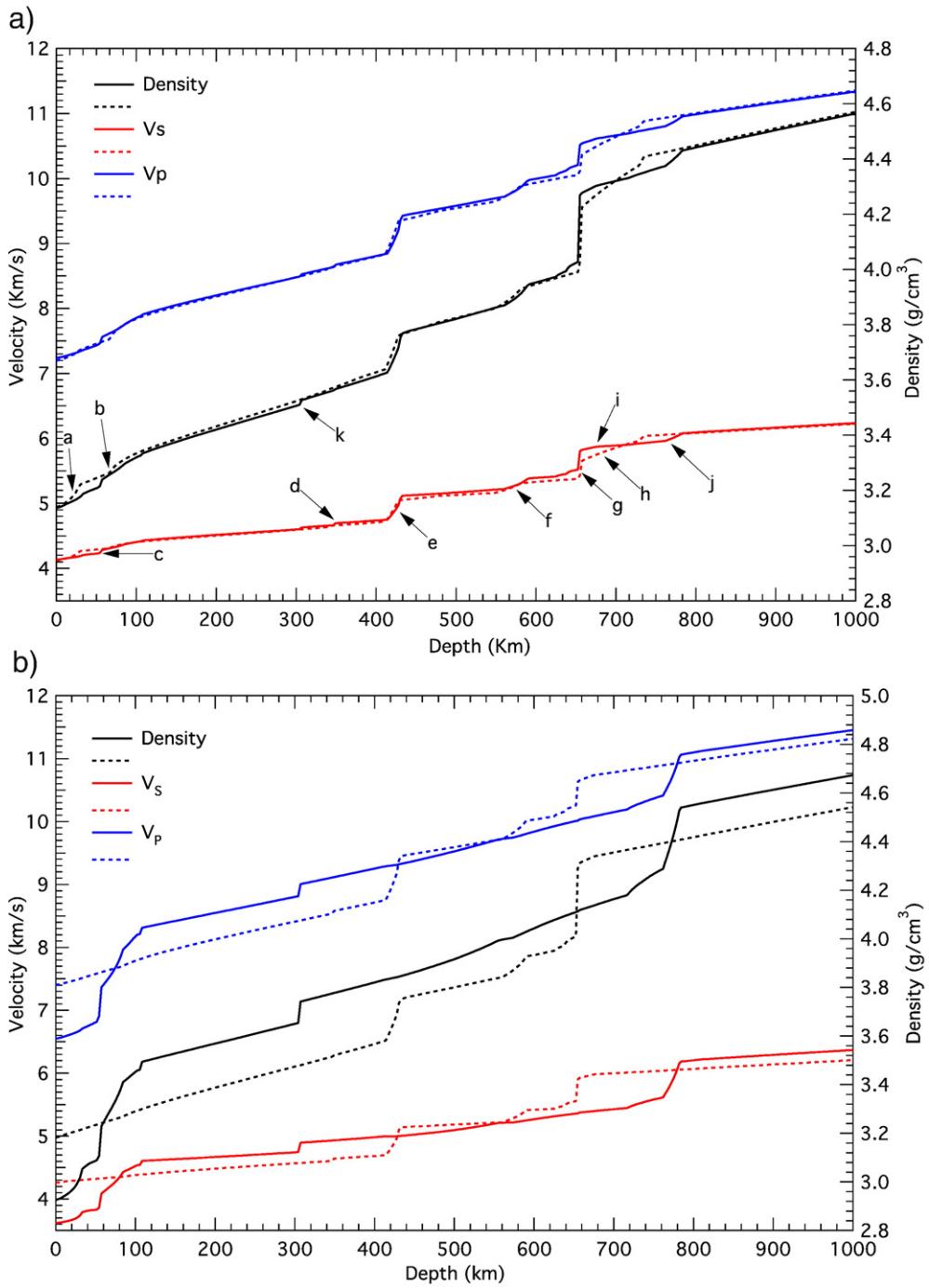

Fig. 3. (top) Seismic wave velocity and density as function of pressure for the mechanical mixture (solid line, denoted as MM) and equilibrium assemblage (dashed line, denoted as EA) along an adiabat with potential temperature 1600 K for identical bulk compositions (basalt fraction 18.02%). The letters label the following phase transformations, which occur in both EA and MM unless otherwise noted: a) plg=sp (EA); b) sp=gt (EA); c) plg=gt (MM); d) opx=C2/c; e) ol=wa; f) wa=ri; g) ri=pv+fp; h) gt=pv (EA); j) gt=pv+capv+st+cf (MM); k) coes=st (MM). (bottom) Seismic wave velocity and density as a function of pressure for the basalt (solid) and harzburgite (dashed) compositions of Table 1.

longer stable (Fig. 2). The velocity gradient directly below the 410 km discontinuity is significantly influenced by the phase change of cpx to garnet. The character of the deep transition zone and the "660" km discontinuity change as the assemblage garnet+ferropericlase is stabilized at the expense of wadsleyite and ringwoodite with increasing basalt fraction for $f>0.3$.

The results are very different in MM (Fig. 5). V_S increases with basalt fraction in the intervals 80–420 km depth and deeper than 770 km, and decreases with basalt fraction elsewhere. This is due to the presence and increasing proportion of stishovite with increasing basalt content; and to a lesser extent to the decreasing proportion of olivine and the increasing proportion of garnet. In the transition zone, the velocity depends only weakly on basalt fraction ($dV_S/df \sim 0.1$ km s^{-1}). Between 660 km and 770 km depth, the velocity decreases with basalt fraction because the garnet to perovskite transition occurs at a greater depth in basalt than it does in harzburgite. The depths and widths of the major discontinuities near 410 km and 660 km discontinuities are unaffected by variations in f since these are due entirely to transformations occurring in the harzburgite fraction. The 520 km discontinuity is substantially smaller than the 410 or 660-km discontinuities due to the relatively small impedance contrast between wadsleyite and ringwoodite. In MM there are two sharp features at the lower mantle

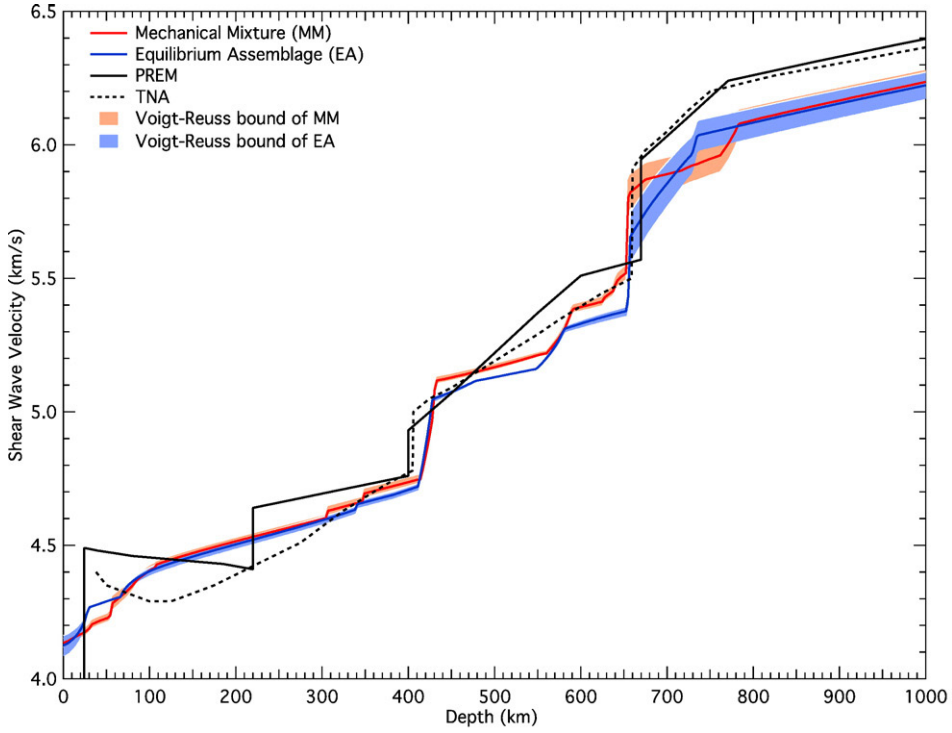

Fig. 4. Shear wave velocity profiles for the two compositional models for identical geotherms and bulk compositions (1600 K and 18.02% basalt fraction). The shading corresponds to the Voigt–Reuss bounds. The bold lines represent the Voigt–Reuss–Hill averages for MM (red) and EA (blue). Black solid line is the PREM profile (Dziewonski and Anderson, 1981) and dashed line TNA (Grand and Helmberger, 1984). (For interpretation of the references to color in this figure legend, the reader is referred to the web version of this article.)

boundary due to the ri=pv+fp transition in the harzburgite component (660 km), and the gt=pv+cf+st transition in the basalt component (770 km).

3.3. Influence of temperature

Temperature influences the velocity of the aggregate via its influence on the elasticity of constituent phases and the phase equilibria (Anderson, 1987; Stixrude and Lithgow-Bertelloni, 2007) (Fig. 6). For example, in regions that are not strongly influenced by phase transformations, the average derivative of velocity with respect to temperature dV_S/dT is similar in EA and MM (-3.4×10^{-4} km s^{-1} K^{-1} and -3.0×10^{-4} km s^{-1} K^{-1} at 200 km and 800 km, respectively). Temperature modifies the depths of the olivine to wadsleyite and ringwoodite to perovskite and ferropericlase transitions. These transitions occur at, respectively, deeper and shallower depths with increasing temperature, reflecting the opposite signs of the effective Clapeyron slopes. In the vicinity of phase transformations, the temperature derivatives vary rapidly and are very different in MM and EA.

The range of temperature explored reveals three significant aspects of the phase equilibria as they influence the velocity structure. First, is the appearance of a double 660 km discontinuity at the lowest temperatures explored: the velocity increase at this discontinuity occurs in two sub-equal steps, separated in depth by approximately 10 km. These two steps are due to the following sequence of transformations: ri=ak+fp, ak=pv, which occur only at low temperature where akimotoite is favored at the expense of garnet. This double step feature is much more pronounced in EA than in MM. In addition to these sharp transitions is a high gradient zone immediately beneath the 660 km discontinuity due to the garnet to perovskite transition, which is present in EA. This feature becomes broader with increasing temperature, and replaces the sharp "660" at the highest temperatures explored. In MM a sharp transition occurs near 770 km at the highest temperatures explored due to the reaction gt=pv+capv+cf+st, which becomes more prominent and sharper at higher temperature. The structure of the 660 km "discontinuity" may be quite complex and the structure that we find may be consistent with seismological observations of a "doubled" 660 km discontinuity (Deuss et al., 2006; Lawrence and Shearer, 2006; Simmons and Gurrola, 2000) or observations of a discontinuity at depths greater than 700 km (Revenaugh and Jordan, 1991a). Second, are increases in the sharpness and magnitude of the 520 km discontinuity with decreasing temperature. The increase in magnitude is due to the reactions gt=wa+st and gt=ri+st which increase the proportion of the olivine polymorphs that produce the 520 km discontinuity. The increase in sharpness is due to a narrowing of the wa=ri phase loop. These temperature-induced variations in the structure of the 520 km discontinuity may explain why it is difficult to observe globally (Shearer, 1996; Lawrence and Shearer 2006). Third, is the transformation of ringwoodite to garnet and ferropericlase that occurs in the deep transition zone at the highest temperatures explored in EA and MM, which influences the velocity gradient and the structure of the "660". The magnitude of the 410 km discontinuity is essentially independent of temperature in both MM and EA except for the very highest temperature. For both MM and EA the width decreases with increasing temperature as expected (Helffrich and Bina, 1994; Stixrude, 1997).

4. Discussion and conclusions

The notion of a mechanical mixture suggests a natural metric for exploring compositional heterogeneity in the mantle. Many previous studies have focused on lateral or radial variations in the relative proportions of iron to magnesium, or of silicon to magnesium (Anderson, 1989; Jeanloz and Knittle, 1989; Stixrude et al., 1992; Trampert et al., 2004). However, such chemical variations are explored in a largely ad-hoc fashion while the processes that might produce them are uncertain. The advantage of basalt fraction as a compositional metric is that the genetic process is well known:

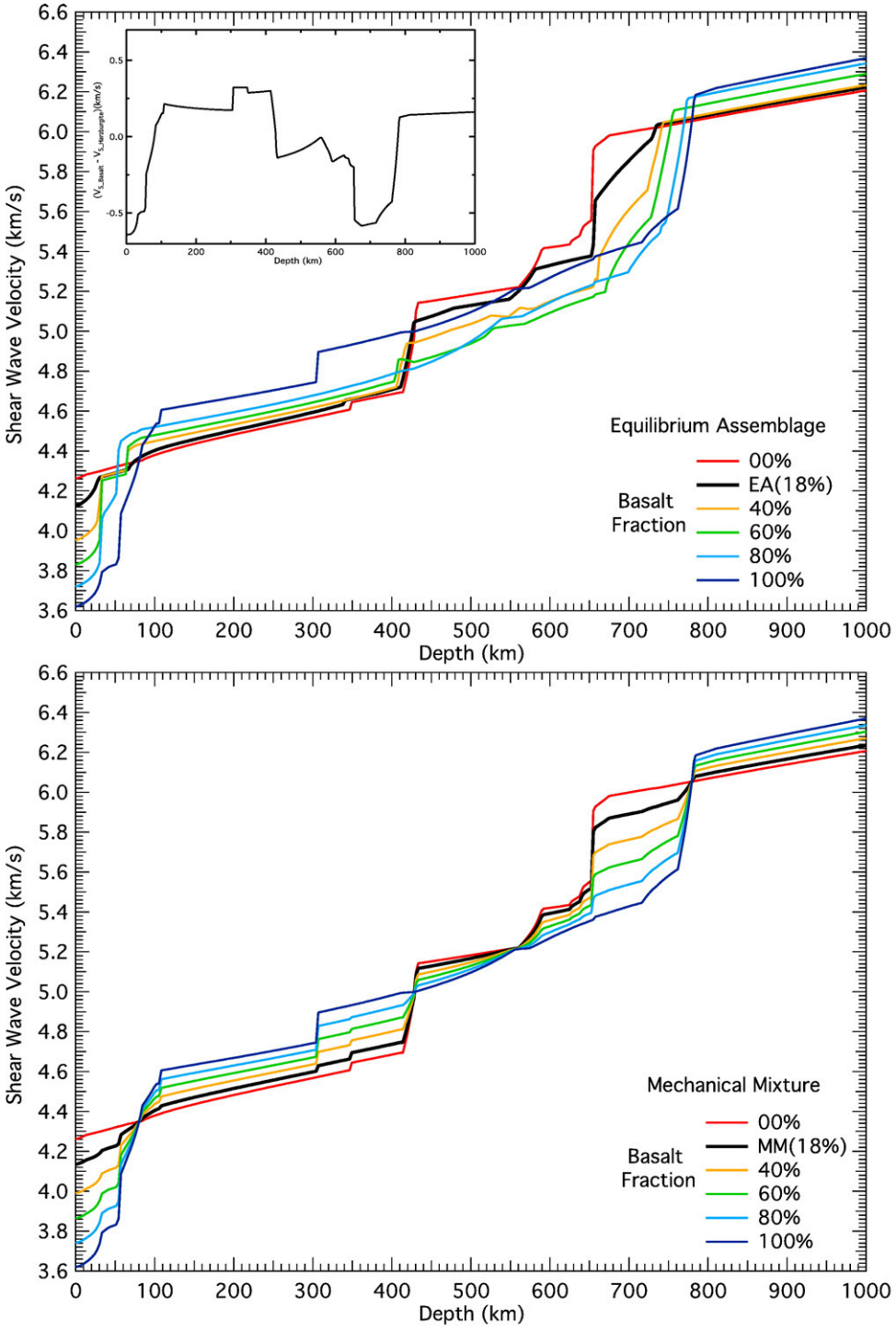

Fig. 5. Profile of shear wave velocity V_S as a function of depth with different basalt fractions (0–100%) for the two models: (Top) mechanical mixture and (bottom) equilibrium assemblage. All calculations are along the 1600 K adiabat of EA pyrolite. The inset shows the velocity difference (V_S) between basalt and harzburgite along the same adiabat.

subduction of differentiated oceanic lithosphere. Moreover, dynamical mechanisms have been proposed for segregating basalt from harzburgite in a convecting mantle, including slab delamination, and segregation due to the density contrast between basalt and harzburgite (Brandenburg and Van Keken, 2007; Christensen and Hofmann, 1994; Davies, 2006; Nakagawa and Buffett, 2005; Ringwood and Irifune, 1988; Xie and Tackley, 2004). Segregation of basalt from harzburgite provides a mechanism for producing radial and lateral variations in basalt fraction.

Within our present understanding of subduction and the differentiated structure of the oceanic lithosphere, it is inevitable that some amount of unequilibrated basalt and harzburgite is present in the mantle. In our mechanical mixture model, we have explored the end-member case, corresponding to a mantle that has undergone differentiation at least once, and in which equilibration is slow compared to the age of the Earth. Does the mantle lie nearer to this mechanically mixed disequilibrium end-member, or to the equilibrium pyrolitic end-member? Arguments based on experimentally measured chemical diffusivities, suggest that equilibration will not be significant over the age of the Earth for the amount of stretching and folding that can be expected in a convecting mantle (Allégre and Turcotte, 1986). However, important uncertainties remain: how much

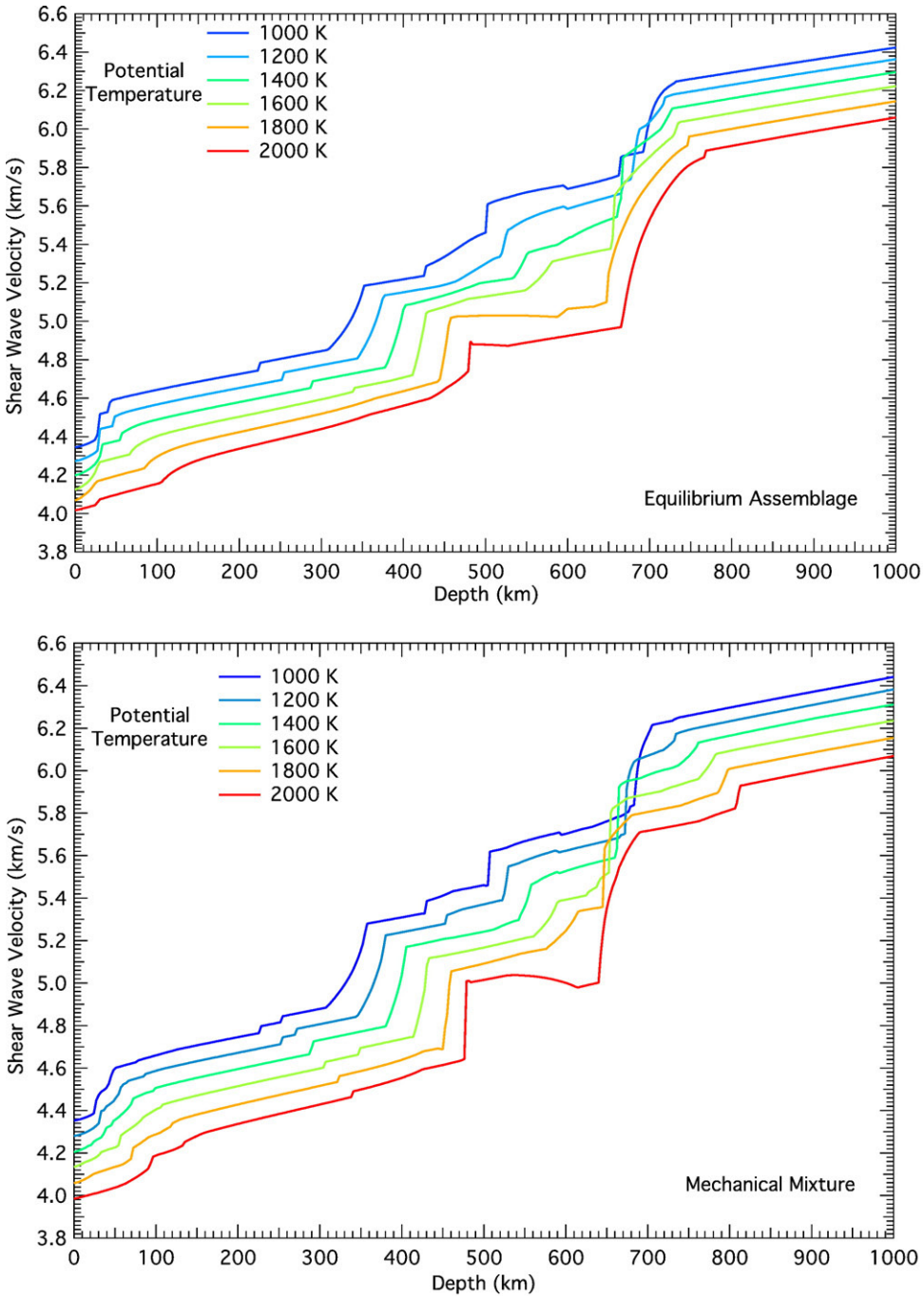

Fig. 6. Shear wave seismic velocity profiles along adiabats of different potential temperatures (1000 K–blue to 2000 K (red) for (top) MM and (bottom) EA. The bulk composition of the two models is identical (f=18.02%). The adiabatic temperature profiles along which the velocities are calculated are computed for EA pyrolite. (For interpretation of the references to color in this figure legend, the reader is referred to the web version of this article.)

of the mantle has been differentiated? What is the basalt fraction? What might the role of partial melt, water, or grain-size reduction be in enhancing rates of equilibration?

Our results provide a means of testing in situ the extent of major element disequilibrium in the mantle based on the significant differences in seismic velocity structure between the equilibrium assemblage and the mechanical mixture. We argue that the mechanical mixture provides a better match to radial seismological models in the transition zone because it is faster and has a steeper radial velocity gradient.

Comparison to radial seismological models provides tentative evidence of a radial gradient in basalt fraction. Whereas the mechanical mixture matches 1D seismological models of the transition zone significantly better than the equilibrium assemblage, the mechanical mixture is almost certainly too fast in the upper mantle, and too slow in the lower mantle, even accounting for uncertainties in seismological models and the effects of lateral heterogeneity. Our results show that basalt depletion in the upper mantle, and basalt enrichment in the lower mantle, would yield better agreement with seismological models by producing a slower upper mantle and a faster lower mantle. Indeed, just such an enrichment in basalt with increasing depth is seen in several models of mantle convection (Davies, 2006; Nakagawa and Buffett, 2005; Xie and Tackley, 2004). Any investigation of the seismological signature of basalt enrichment

or other compositional metrics must take into account the variation in sign and magnitude with depth of the compositional derivative (dV/df, Fig. 5), rather than assuming the derivatives are independent of depth as in previous geophysical studies (e.g. Forte and Mitrovica, 2001; Trampert et al., 2004).

Our results suggest a powerful thermometer of the transition zone. A remarkable feature of the mechanical mixture model is that the velocity in the transition zone is nearly independent of bulk composition. If this model is representative of the mantle, seismic velocities will be primarily sensitive to temperature. Comparison of the absolute velocity of the mechanical mixture model to that constrained seismically in the transition zone should provide an independent means of determining mantle temperature at depth.

Our results may permit tests of the nature and length scale of lateral variations in composition. We predict that discontinuity structure will vary laterally with both temperature and composition, in ways that are distinct for EA and MM end-members, so that it would be best explored at a regional level, in areas where the tectonic history of the mantle is well known. A mechanically mixed mantle should also produce scattering due to the significant velocity contrast between basalt and harzburgite (Stixrude and Jeanloz, 2007).

The apparent discrepancy between the magnitude of the 410 km discontinuity in MM and EA vs. that in seismological models may be due to the finite frequency of seismic waves (Jackson, 2008). In the case of EA this apparent discrepancy has been recognized before and has formed the basis for proposing olivine-depleted models of mantle composition in which the magnitude of the 410 is reduced and in better agreement with seismology (Duffy et al., 1995). In MM the magnitude of the 410 km discontinuity is even greater than it is in EA. However, our calculations, like previous ones, assumed that the frequency of the elastic wave is sufficiently high that its passage does not excite transformation of olivine to wadsleyite. This assumption may not be valid. To the extent that partial transformation does occur at seismic frequencies, the wave velocity will be reduced, which should help to explain the smaller magnitudes of the 410 km discontinuity seen in seismological models, although at present it is not possible to quantify this effect further because of uncertainties in the rate of grain growth at seismic frequencies.

Appendix A. Supplementary data

Supplementary data associated with this article can be found, in the online version, at doi:10.1016/j.epsl.2008.08.012.

References

Allégre, C.J., Turcotte, D.L., 1986. Implications of a two-component marble-cake mantle. Nature 323, 123–127.

Anderson, D.L., 1987. Thermally induced phase-changes, lateral heterogeneity of the mantle, continental roots, and deep slab anomalies. J. Geophys. Res.-Solid Earth Planets 92, 13968–13980.

Anderson, D.L., 1989. Theory of the Earth. Blackwell Scientific Publications, Boston, pp. 147–177.

Anderson, D.L., Bass, J.D., 1986. Transition region of the earth upper mantle. Nature 320, 321–328.

Baker, M.B., Beckett, J.R., 1999. The origin of abyssal peridotites: a reinterpretation of constraints based on primary bulk compositions. Earth Planet. Sci. Lett. 171, 49–61.

Bass, J.D., 1995. Elasticity of minerals, glasses, and melts, in mineral physics and crystallography. In: Ahrens, T.J. (Ed.), A Handbook of Physical Constants. AGU, Washington, D.C., p. 465-463.

Brandenburg, J.P., Van Keken, P.E., 2007. Deep storage of oceanic crust in a vigorously convecting mantle. J. Geophys. Res. 112, B06403. doi:10.1029/2006JB004813.

Callen, H.B., 1960. Thermodynamics. John Wiler & Sons, New York.

Chen, C.Y., Frey, F.A., Garcia, M.O., et al., 1991. The tholeiite to alkalic basalt transition at Haleakala Volcano, Maui, Hawaii. Contrib. Mineral. Petrol. 106, 183–200.

Christensen, U., Hofmann, A.W., 1994. Segregation of subducted oceanic crust in the mantle. J. Geophys. Res. 99, 19867–19884.

Davies, G.F., 2006. Gravitational depletion of the early Earth's upper mantle and the viability of early plate tectonics. Earth Planet. Sci. Lett. 243, 376–382.

Deuss, A., Redfern, S.A.T., Chambers, K., et al., 2006. The nature of the 660-kilometer discontinuity in earth's mantle from global seismic observations of PP precursors. Science 311, 198–210.

Duffy, T., Zha, C.S., Downs, R.T., et al., 1995. Elasticity of forsterite to 16 GPa and the composition of the upper mantle. Nature, 378, 170–173.

Dziewonski, A.M., Anderson, D.L., 1981. Preliminary reference Earth model. Phys. Earth Planet. Inter. 25, 297–356.

Farber, D.L., Williams, Q., Ryerson, F.J., 1994. Diffusion in Mg_2SiO_4 polymorphs and chemical heterogeneity in the mantle transition zone. Nature 371, 693–695.

Forte, A.M., Mitrovica, J.X., 2001. Deep-mantle high-viscosity flow and thermochemical structure inferred from seismic and geodynamic data. Nature 410, 1049–1056.

Francis, D., 1987. Mantle-melt interaction recorded in spinel lherzolite xenoliths from the Alligator lake Volcanic complex, Yukon, Canada. J. Petrol. 28, 569–597.

Frey, F.A., Green, D.H., Roy, S.D., 1978. Integrated models of basalt petrogenesis: a study of Quartz Tholeiites to Olivine melilitites from south eastern Australia utilizing geochemical and experimental petrological data. J. Petrol. 19, 463–513.

Grand, S.P., Helmberger, D.V., 1984. Upper mantle sheart structure of North America. Geophys. J. Roy. Astron. Soc. 76, 399–438.

Green, D.H., Hibberson, W.O., Jaques, A.L., 1978. In: McElhinny, M.W. (Ed.), Petrogenesis of Mid-Ocean Ridge Basalts in The Earth, its Origin, Structure and Evolution. Academic Press, London, pp. 255–299.

Helffrich, G., Bina, C.R., 1994. Frequency-dependence of the visibility and depths of mantle seismic discontinuities. Geophys. Res. Lett. 21, 2613–2616.

Hirschmann, M.M., Stolper, E.M., 1996. A possible role for garnet pyroxenite in the origin of the “garnet signature” in MORB. Contrib. Mineral. Petrol. 124 (2), 185–208.

Hoffman, A.W., Hart, S.R., 1978. Assessment of local and regional isotopic equilibrium in the mantle. Earth Planet. Sci. Lett. 38, 44–62.

Irifune, T., 1993. Phase transformation in the earth's mantle and subducting slabs: implications for their compositions, seismic velocity and density structures and dynamics. Island Arc 2, 55–71.

Ito, E., Sato, H., 1991. Aseismicity in the lower mantle by superplasticity of the descending slab. Nature 351, 140–141.

Ita, J.J., Stixrude, L., 1992. Petrology, elasticity and composition of the transition zone. J. Geophys. Res. 97, 6849–6866.

Jackson, I., 2008. Properties of rocks and minerals — physical origins of anelasticity and attenuation in rock. In: Schubert, G. (Ed.), Treatise on Geophysics. Mineral Physics, vol. 2. Elsevier, Amsterdam, pp. 493–525.

Jeanloz, R., Knittle, E., 1989. Density and composition of the lower mantle. Philos. Trans. R. Soc. Lond. 328, 377–389.

Kellogg, J.B., Jacobsen, S.B., O'Connell, R.J., 2002. Modeling the distribution of isotopic ratios in geochemical reservoirs. Earth Planet. Sci. lett. 204, 183–202.

Lawrence, J.F., Shearer, P.M., 2006. Constraining seismic velocity and density for the mantle transition zone with reflected and transmitted waveforms. Geochem. Geophys. Geosyst. 7, Q10012. doi:10.1029/2006GC001339.

Mattern, E., Matas, J., Ricard, Y., Bass, J., 2005. Lower mantle composition and temperature from mineral physics and thermodynamic modelling. Geophys. J. Int. 160 (3), 973–990.

McKenzie, D., Bickle, M.J., 1988. The volume and composition of melt generated by extension of the lithosphere. J. Petrol. 29, 625–679.

Morgan, J.P., Morgan, W.J., 1999. Two-stage melting and the geochemical evolution of the mantle: a recipe for mantle plum-pudding. Earth Planet. Sci. Lett. 170 (3), 215–239.

Nakagawa, T., Buffett, B.A., 2005. Mass transport mechanisms between the upper and lower mantle in numerical simulations of thermo-chemical mantle convection with multi-component phase changes. Earth Planet. Sci. Lett. 230, 11–27.

Presnall, D.C., Hoover, J.D., 1987. In: Mysen, B.O. (Ed.), High-Pressure Phase Equilibrium Constraints on the Origin of Mid-Ocean Ridge Basalts in Magmatic Processes: Physical Chemical Principles. Special Pub. Geochem. Soc., vol. 1, pp. 75–89.

Revenaugh, J., Jordan, T.H., 1991a. Mantle layering from ScS reverberations 2. The transition zone. J. Geophys. Res.-Solid Earth 96, 19,763–19,780.

Revenaugh, J., Jordan, T.H., 1991b. Mantle layering from ScS reverberations 3. The upper mantle. J. Geophys. Res.-Solid Earth 96, 19,781–19,810.

Ringwood, A.E., 1966. The chemical composition and origin of the earth. In: Hurley, P.M. (Ed.), Advances in Earth Science. M.I.T. Press, Cambridge, Mass., pp. 287–356.

Ringwood, A.E., 1969. Composition and evolution of the upper mantle. In: Hart, P.J. (Ed.), The Earth's Crust and Upper Mantle: Structure, Dynamic Process, and their Relations to Deep-Seated Geological Phenomena. Geophys. Mongr. Ser., vol. 13, pp. 1–17. Washington, D. C.

Ringwood, A.E., 1979. Origin of the Earth and Moon. Springer-Verlag New York, Inc, New York.

Ringwood, A.E., Irifune, T., 1988. Nature of the 650-km seismic discontinuity: implications for mantle dynamics and differentiation. Nature 331, 131–136.

Shearer, P.M., 1996. Transition zone velocity gradients and the 520-km discontinuity. J. Geophys. Res. 101, 3053–3066.

Simmons, N.A., Gurrola, H., 2000. Multiple seismic discontinuities near the base of the transition zone in the Earth's mantle. Nature 405, 559–562.

Sobolev, A.V., Hofmann, A.W., Kuzmin, D.V., et al., 2007. The amount of recycled crust in sources of mantle-derived melts. Science 316, 412–417.

Stixrude, L., 1997. Structure and sharpness of phase transitions and mantle discontinuities. J. Geophys. Res.-Solid Earth 102, 14835–14852.

Stixrude, L., Jeanloz, R., 1990. Constraints on seismic models from other disciplines – Constraints from mineral physics on seismological models, in Treatise on Geophysic. In: Schubert, G. (Ed.), Seismology and the Structure of the Earth, vol. 1. Elsevier Ltd., Oxford, pp. 775–803. doi:10.1016/B978-044452748-6/00026-2.

Stixrude, L., Lithgow-Bertelloni, C., 2005a. Mineralogy and elasticity of oceanic upper mantle: Origin of the low velocity zone. J Geophys. Res. 110, B03204. doi:10.1029/2004JB002965.

Stixrude, L., Lithgow-Bertelloni, C., 2005b. Thermodynamics of mantle minerals I: physical properties. Geophys. J. Int. 162, 610–632.

Stixrude, L., Lithgow-Bertelloni, C., 2007. Influence of phase transformations on lateral heterogeneity and dynamics in Earth's mantle. Earth Planet. Sci. Lett 263, 45–55.
Stixrude, L., Hemley, R.J., Fei, Y., Mao, H.K., 1992. Thermoelasticity of silicate perovskite and Magnesiowüstite and stratification of the earth's mantle. Science 257, 1099–1101.
Trampert, J., Deschamps, F., Resovsky, J., Yuen, D., 2004. Probabilistic tomography maps chemical heterogeneities throughout the lower mantle. Science 306, 853–856.
Watt, J.P., Davies, G.F., O'Connell, R.J., 1976. The elastic properties of composite materials. Rev. Geophys. Space Phys. 14, 541–563.
Weidner, D.J., 1985. A mineral physics test of a pyrolite mantle. Geophys. Res. Lett. 12, 417–420.
Williams, Q., Revenaugh, J., 2005. Ancient subduction, mantle eclogite, and the 300 km seismic discontinuity. Geology 33 (1), 1–4.
Woodland, A.B., 1998. The orthorhombic to high-p monoclinic phase transition in Mg–Fe pyroxenes: can it produce a seismic discontinuity? Geophys. Res. Lett. 25, 1241–1244.
Workman, R.K., Hart, S.R., 2005. Major and trace element composition of the depleted MORB mantle (DMM). Earth Planet. Sci. Lett. 231, 53–72.
Xie, S., Tackley, P., 2004. Evolution of U–Pb and Sm–Nd systems in numerical models of mantleconvection and platetectonics. J. Geophys. Res. 109. doi:10.1029/2004JB003176.
Xu, X., Lithgow-Bertelloni, C., Conrad, C.P., 2006. Global reconstructions of Cenozoic seafloor ages: implications for bathymetry and sea level. Earth Planet. Sci. Lett. 243, 552–564.
Yamazaki, D., Kato, T., Yurimoto, H., et al., 2000. Silicon self-diffusion in $MgSiO_3$ perovskite at 25 GPa. Phys. Earth Plant. Inter. 119, 299–309.